Lab on a Chip

Cite this: *Lab Chip*, 2012, **12**, 1963–1966

www.rsc.org/loc

COMMUNICATION

Contactless conductivity biosensor in microchip containing folic acid as bioreceptor†‡

Renato S. Lima,[ab] Maria H. O. Piazzetta,[c] Angelo L. Gobbi,[c] Ubirajara P. Rodrigues-Filho,[a] Pedro A. P. Nascente,[d] Wendell K. T. Coltro[be] and Emanuel Carrilho*[ab]

Received 13th February 2012, Accepted 17th April 2012
DOI: 10.1039/c2lc40157f

We report a glass/PDMS-based microfluidic biosensor that integrates contactless conductivity transduction and folic acid, a target for tumor biomarker, as a bioreceptor. The device presents relevant advantages such as direct determination—dismiss the use of redox mediators as in faradaic electrochemical techniques—and the absence of the known drawbacks related to the electrode-solution interface. Characterizations of the functionalization processes and chemical sensor are described in this communication.

To capture exogenous folic acid (FA)—an oxidized and non-physiological species of vitamin B—animal cells possess at their surface folate receptors (FR), which bind FA with high affinity (association constants in the order of 10^9 to 10^{10}) at 1 : 1 stoichiometry. A homology search of the human genome revealed four distinct FR genes, termed: FR-α, -β, -γ, and -δ. FR-α is an extracellular tumor biomarker which is present under elevated expression levels in cancer cells arising from the glandular tissue in ovary, uterus, and cervix. The highest expression of FR-α is associated with poorly differentiated and more aggressive tumors. Such aspects assist in the implementation of future therapeutic actions and allow the monitoring of the cancer in order to evaluate curative effects.[1] A few reports have demonstrated the use of FA as a bioreceptor in biosensors for detection of FR-α. Cyclic voltammetry,[2] atomic force microscopy (AFM),[3] diffraction,[4] and impedance[5] are transduction techniques used so far. These studies showed the potential use of FA-based biosensors for FR-α in blood samples, obtained from patients with different types of cancer.

Lab-on-a-chip (LOC) platforms for cancer biomarker detection have been reported in the literature and it is subject of great interest.[6–10] LOC systems carry important advantages, including: *i*) reduced chemical consumption, *ii*) high analytical frequency, and *iii*) great device portability.[11] Such factors are essential to the development of point-of-care methods, capable of processing samples in the field (as ambulances, clinics, and patient's homes) for analysis of different biomarkers.[12]

Faradaic electrochemical methods are the most widely used in biosensors due to the following factors: *i*) they require low cost instrumentation, *ii*) they present good sensitivity, *iii*) they are non-destructive, and *iv*) they exhibit high integration (co-fabrication of electrodes in microdevices). On the other hand, the main limitation of these devices originates from the contact between the electrode and sample, generating drawbacks such as: *i*) fouling of the electrodes, *ii*) non-uniformity of the surface, and *iii*) interference between the detector circuitry and the high electric field when applied in electrophoresis systems. A potential alternative is the capacitively coupled contactless conductivity detection (C^4D) technique, which has been widely employed for diverse analytical determinations over the last ten years.[13]

In biosensor-based analytical systems, the specificity is mainly governed by the bioreceptor/ligand interactions so that universal transducers such as C^4D can be employed.[14] Recently, Coltro *et al.*[15] reported the use of the C^4D as a new transducer in microchips for biomolecular interactions analysis (named as μBIA-C^4D). Herein we describe the development, optimization, and characterization of this platform containing FA as a bioreceptor, which represents a promising method aimed at FR-α biomarker detection.

The C^4D microfluidic device consisted of PDMS (with the molded microchannels) and glass (with the electrodes and the insulating dielectric). Fig. 1 shows the constituent layers and a photo of the microsystem. Briefly, the microchannels of 250 μm width and 50 μm depth were molded in a Y-shape using soft lithography. The electrodes, in turn, were sputter-deposited (layered as Ti/Au/Ti) presenting 1.0 mm of width and gap. For electric insulation of the electrodes, a thin film SiO_2 with 50 nm thickness was deposited by plasma-enhanced chemical vapor deposition (PECVD) (studies about the optimization of the dielectric thickness are described in

[a]*Instituto de Química de São Carlos, Universidade de São Paulo, São Carlos, SP, Brazil. E-mail: emanuel@iqsc.usp.br; Fax: +55 (16) 3373 9975; Tel: +55 (16) 3373 9441*
[b]*Instituto Nacional de Ciência e Tecnologia de Bioanalítica, Campinas, SP, Brazil*
[c]*Laboratório Nacional de Nanotecnologia, Centro Nacional de Pesquisa em Energia e Materiais, Campinas, SP, Brazil*
[d]*Departamento de Engenharia de Materiais, Universidade Federal de São Carlos, São Carlos, SP, Brazil*
[e]*Instituto de Química, Universidade Federal de Goiás, GO, Goiânia, Brazil*
† Published as part of a themed issue in collaboration with the III International Workshop on Analytical Miniaturization and NANOtechnologies, Barcelona, 2012.
‡ Electronic supplementary information (ESI) available: Materials and methods, effect of the area on the response in C^4D, optimization of the dielectric thickness and silanization conditions, and details about the FA-functionalization protocol. See DOI: 10.1039/c2lc40157f

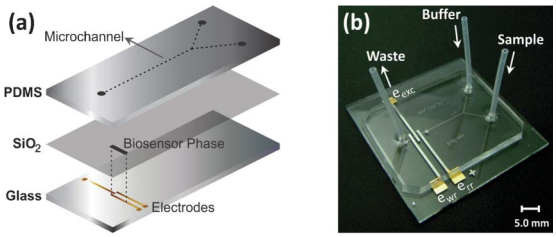

Fig. 1 Scheme for μBIA-C^{4}D. Expanded view of the layers that compose the microchip (a) and photo of the microchip (b). e_{exc} is the excitation electrode, and e_{rr} and e_{wr} are the reference and working receiver electrodes, respectively.

Fig. S1, ESI‡). Before the sealing step, the PDMS surface was oxidized in O_2 plasma for 13 s. Then, the plates were put in contact ensuring an irreversible process.[16]

The μBIA-C^{4}D carries three electrodes; besides an excitation electrode (e_{exc}), in which the alternating signal is applied, there are two receiver electrodes, reference (e_{rr}) and working (e_{wr}) receiver electrodes. Only the dielectric surface over e_{wr} was functionalized. Fig. 2 shows a closer view of the microfluidic channel in the detection zone. For the analyses of biomolecular interactions, conductivity measurements were carried out in real time while either buffer or analyte solution was flowing through the microfluidic channels driven by two external syringe pumps. First, the buffer flushed the channels for approximately five min for stabilization of the signal and definition of the baseline. Afterwards, samples were introduced generating a response change on both receiver electrodes. The e_{rr} signal (S_r) correlates to the conductivity of the electrolytic medium, while the e_{wr} signal (S_w) also responds to the bioreceptor/ligand interactions. Consequently, the $S_w - S_r$ difference is closely related to the biomolecular interactions. We hypothesize that this signal arises from raising of the biosensing area when the biointeractions occur, along with changes in the dielectric constant. This phenomenon should increase the output voltage recorded by e_{wr} (discussed in the ESI‡). Finally, after a specific time (sampling time), the buffer was added again for regeneration of the biosensor phase. As consequence, there was a decrease of the signal nearly to its initial value. The $S_w - S_r$ value obtained at the end of the sampling time represents the analytical response in μBIA-C^{4}D. All measurements were taken at room temperature. In this study, we performed the commutation

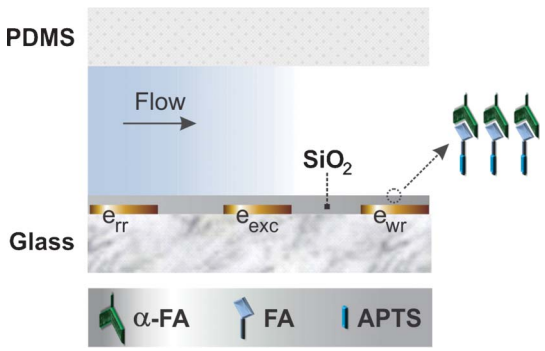

Fig. 2 Detailed scheme of the microchannel with electrode setup and structure in the μBIA-C^{4}D detection zone. APTS, FA, and α-FA are 3-(aminopropyl)triethoxysilane (immobilization intermediary), folic acid (bioreceptor), and monoclonal antibody to the FA (ligand), respectively. Other parameters are defined in Fig. 1.

of the syringe pumps manually. Meanwhile, for high precision tests, software-controlled valves could be used.

For silanization of the surface of the SiO_2 film, the silanes 4-(triethoxysilyl)butyronotrile (ButCN) and 3-(aminopropyl) triethoxysilane (APTS) were investigated as intermediaries for immobilization of FA by formation of self-assembly monolayers (SAMs) on the SiO_2 dielectric film. Table S1 (ESI‡) summarizes the parameters used in the assays—solvent, reagent concentration, and reaction time—which were intended to optimize the silanization conditions. Excessive concentrations and long reaction times can generate two artifacts: *i*) condensation in the solvent phase and *ii*) polymerization of the silane on the substrate surface. The first generates oligomers and/or polymers, which are adsorbed on the substrate surface. The second, in turn, arises from condensations between the silanol groups (Si–OH) of the silane.[17] Both phenomena produce colloidal clusters on the substrate, inhibiting the formation of organized, reproducible, dense, and smooth silane layers. Low concentrations and short reaction times, on the other hand, reduce the fractional coverage of the surface by the silane.[18]

The silane-modified surfaces were characterized by taking scanning electron microscopy (SEM) and X-ray photoelectron spectroscopy (XPS) measurements. SEM was used for checking the formation of clusters. XPS was employed for qualitative and quantitative determinations of the silanized surfaces, allowing us to ascertain the adsorption rate of the silanes.[19]

For all conditions investigated in this paper, the SEM images did not indicate clustering to 3 μm, 1 μm, and 200 nm resolution levels (Fig. S2, ESI‡). These results can be attributed to the low hydration degree of the SiO_2 films deposited by PECVD (as the XPS measures confirmed). This fact prevents the formation of protonated species in silanization reactions, which arise from interactions between the organofunctional groups of the silane and silanol groups present on hydrated substrate surfaces. Such species favor homogeneous polymerizations with subsequent deposition of colloidal clusters, as described earlier.

Concerning the XPS assays, the chemical compositions of the films were elucidated as previously reported.[19–23] The Si 2p peaks for all modified samples were fitted with only one component, the Si–O bond from SiO_2 (about 103.3 eV, Fig. S3, ESI‡). Additionally, measures of a non-modified sample resulted in the same setting for the Si 2p peak. This fact confirms the low hydration degree of the SiO_2 substrate given the absence of the Si–OH component (about 99.6 eV). The N 1s peak showed asymmetric line shapes being fitted with three components (Fig. S4a–c, ESI‡); two of them correspond to the species Si_3N_4 (about 398.6 eV) and N–C (about 400.4 eV). The third spectral line refers to NH_3^+ (about 401.7 eV) and NO_2^- (about 403.2 eV) for APTS- and ButCN-modified samples, respectively. The N–C component indicates the presence of silane, whereas Si_3N_4 and NO_2^- can be attributed to the dielectric deposition by PECVD. This process generates nitrogen as a product of the reactions in plasma.[24] Finally, the NH_3^+ component is assigned to interactions involving silanol groups present in the substrate and the $–NH_2$ groups of the APTS (Fig. S5, ESI,‡ shows the APTS-silanization mechanism on a SiO_2 surface, followed by the APTS-FA reaction).[19]

From the XPS semi-quantitative analyses, it was possible to calculate the N/Si atomic ratios. For this, the N–C N 1s (characterizes the formation of silane) and Si–O Si 2p (inherent to the substrate nature) components were considered.[19] Fig. S4d (ESI‡) illustrates the obtained

N/Si ratios, which was highest for the following conditions: 3% (v/v) APTS in ethanol and 300 min of reaction time. Thus, such parameters were used in subsequent analyses.

After optimization of the silanization conditions, the FA-functionalization step was investigated. For this, the experimental protocol reported by Bhalerao *et al.*[3] was employed (described in detail in the ESI‡). Prior to the biointeraction assays, absolute values of the baseline potential (V_B) in C^4D were obtained by filling the microchip with 100 mmol L^{-1} MES at pH 2.3 (buffer used in the biomolecular studies). This experiment aimed to select the ideal transduction parameters, namely: frequency (kHz) and peak-to-peak voltage ($V_{P\text{-}P}$). Fig. 3a expresses variations of V_{BL} in function of the frequency under the potentials: 2.5, 6.0, and 9.5 $V_{P\text{-}P}$. The results were similar to those obtained with the polyester-toner C^4D microchip.[25] There is a maximum V_B (V_B^{max}) indicating the optimum value of the working frequency. This point is shifted to lower frequencies with the increase of the peak-to-peak voltage. For 2.5, 6.0, and 9.5 $V_{P\text{-}P}$, the V_B^{max} levels were recorded at 340, 220–300, and 180–260 kHz, respectively. Since the raising of the potential from 6.0 to 9.5, $V_{P\text{-}P}$ did not result in significant variations of V_B^{max} (8.5 to 8.7), the subsequent biomolecular analyses were performed by applying an rf frequency of 300 kHz and a peak-to-peak voltage of 6.0 $V_{P\text{-}P}$. The bioassays were carried out using an antibody specific to FA (α-FA) as a ligand instead of FR-α. The later and circulating tumor cells are not available as analytical standards. Since C^4D is a universal detector, correlation between the binding of α-FA to FA and the signal in μBIA-C^4D could be inferred. Three FA-functionalization times were ascertained, namely: 3, 5, and 7 h, and evaluated the signal intensities obtained by the μBIA-C^4D. Fig. 3b–d show the responses obtained by the μBIA-C^4D microsystems commutating MES buffer (100 mmol L^{-1}, pH 2.3) and α-FA ligand (100 μg mL^{-1} in TBS, pH 7.3) at 20 μL min^{-1} flow rate. The decrease of the analytical signal after the sampling step (30 s) occurred due to regeneration of the biosensor phase, which consisted of breaking the FA–α-FA interactions allowing new biomolecular events for subsequent analysis. The regeneration phenomenon was achieved by denaturation of the α-FA protein using extremes of pH as denaturing agent.[26] The chips obtained with 3 h functionalization presented responses slightly higher than the other reaction times. The μBIA-C^4D signals ($S_w - S_r$) were: 0.7 (3 h), 0.5 (5 h), and 0.4 V (7 h of functionalization). These results may be attributed to a steric factor related to higher functionalization times. Although entailing a greater number of bioreceptor anchors, long reaction times may generate steric hindrances for the bioactive component of these species as a function of the high density of molecules near the surface of the sensor phase.[27] Using the calibration method and assuming that the concentration of 100 μg mL^{-1} is within the dynamic range, the LOD value was calculated as 16.9 μg mL^{-1} of α-FA ligand for 3 h of functionalization. In addition, the devices exhibited good inter- and intra-assay (microfabrication reproducibility) precisions. The percentage relative standard deviations (RSD) of seven measurements for each microchip were: 5.7 (3 h), 7.9 (5 h), and 6.4% (7 h of functionalization). Finally, the inter-assay precision of the device for 3 h FA-functionalization was measured from three assays on different days (same conditions as in Fig. 4b). After seven measurements for each microchip, the RSD was calculated as 13.1%.

As a negative control, in addition to the assays with α-FA using the electrode/SiO_2 (e_{rr}) and electrode/SiO_2/APTS/FA (e_{wr}, functionalization for 3 h) microchips, we measured the C^4D signal of a device incorporating only the immobilization intermediary (electrode/SiO_2/APTS). The results shown in Fig. 4a indicate that there was no difference between the signals from electrode/SiO_2 and electrode/SiO_2/APTS. In such cases there were no specific interactions of the α-FA ligand to the electrodes given the absence of FA. Comparatively, we observed an increase of the response only for the electrode/SiO_2/APTS/FA system. These data indicate

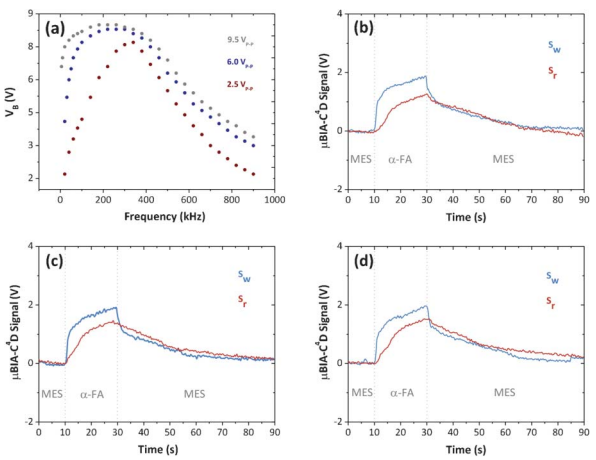

Fig. 3 Optimization of detection parameters and FA-functionalization conditions. Variations of C^4D signal as function of the frequency and potential (a) and responses obtained by μBIA-C^4D using 3 (b), 5 (c), and 7 h (d) of functionalization. V_B is the baseline potential, whereas S_r and S_w are the signals obtained by the reference and working receiver electrodes, respectively. Conditions: 100 mmol L^{-1} MES buffer (pH 2.3), 100 μg mL^{-1} α-FA ligand in TBS (pH 7.3), 20 μL min^{-1} flow rate, 300 kHz frequency, and 6.0 $V_{P\text{-}P}$ peak-to-peak voltage.

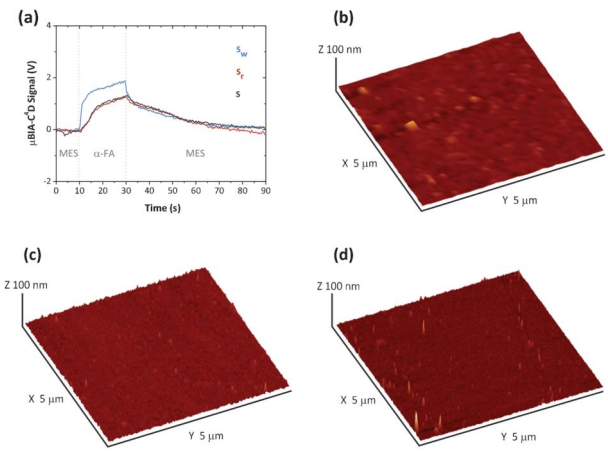

Fig. 4 Characterization of biosensor phase. C^4D measurements involving the electrode/SiO_2, electrode/SiO_2/APTS, and electrode/SiO_2/APTS/FA systems (a) and AFM images of the SiO_2 (b), SiO_2/APTS (c), and SiO_2/APTS/FA (d) surfaces. *S*, signal obtained by the electrode/SiO_2/APTS system. The conditions for figure (a) are described in Fig. 3. The roughness parameters of the surfaces were: *i*) RMS = 0.4 (SiO_2), 0.8 (SiO_2/APTS), and 1.0 nm (SiO_2/APTS/FA); *ii*) SAR = 0.8 (SiO_2), 5.1 (SiO_2/APTS), and 6.3% (SiO_2/APTS/FA); and *iii*) DS = 5,621.7 (SiO_2), 7,055.3 (SiO_2/APTS), and 9,034.6 μm^{-2} (SiO_2/APTS/FA).

a direct correlation between the analytical signal in μBIA-C^4D and the occurrence of biomolecular interactions in real time, showing that the C^4D can be used as transduction technique in chemical and biochemical sensing.

For morphological characterization of the biosensor phase, the SiO_2, SiO_2/APTS, and SiO_2/APTS/FA surfaces were analyzed by AFM. The following parameters were considered: root mean square (RMS), surface-to-area ratio (SAR), and density of summits (DS).[16] The images achieved, as well as the RMS, SAR, and DS values, are shown in Fig. 4b–d. We observed the formation of slightly rougher surfaces and with higher surface area and density of peaks for the sequential process of silanization and functionalization.

This communication reports a potential alternative for determination of species that binds FA with high affinity, including the FR-α cancer biomarker. The biosensing microchip, which integrates contactless conductivity transduction and FA as bioreceptor, exhibits relevant advantages. Among these, we can highlight: *i*) reduced sample and reagent consumption (< 7 μL); *ii*) rapid analyses (< 2 min); *iii*) simple assay routine (commuting 2 syringe pumps); *iv*) cheap and portable instrumentation (home-made electronics under $100); *v*) possibility of fabrication of the chips without use of clean rooms (hundreds of μm features; glass/PDMS sealing); and *vi*) monitoring of the biomolecular interactions in real time (implications in kinetics and thermodynamics of the binding event). The transducer of choice—C^4D—displays two highly positive aspects: *i*) direct determinations, dispensing the use of redox mediators as in faradaic electrochemical methods, and *ii*) absence of drawbacks related to the electrode–solution contact. On the other hand, the levels of detectability achieved by μBIA-C^4D are rather low with such simple instrumentation and can further be improved. The poor sensitivity is an intrinsic drawback to the conductivity-based sensors. The conductivity of a solution is determined by the migration of all ions present. Thus, in complex matrixes like biological samples, the high ionic strength of the medium may mask the net conductivity changes caused by biointeractions.[28] Thus, alternatives for improving the sensitivity of the μBIA-C^4D can be foreseen. Among the options to improve the signal, we can include: *i*) metal nanoparticles,[29–31] which increase the density of active species anchored to biosensor phase, *ii*) high-voltage excitation signals,[32] *iii*) ground plane to reduce the stray capacitance,[32] *iv*) C^4D cells with higher sensing area, such as semicircular [33,34] and dual top-bottom electrodes,[35] and *v*) techniques to raise the signal-to-noise ratio.[36–41] In addition, the doping of the dielectric thin film insulating the electrodes represents another real possibility.[16] The later consists of increasing the dielectric constant of the thin film and, soon, the conductance recorded by the electrodes in C^4D.

This project was financially supported by the Fundação de Amparo à Pesquisa do Estado de São Paulo (FAPESP) (Grants Nr. 2008/07597-4 and 2010/08559-9). The authors are thankful to Msc. Paulo C. Leme and Dr Adriano L. de Souza for their assistance with the surface modification processes. In addition, Vinícius L. Pimentel and Dr Thiago P. Segato are acknowledged for their assistance with the AFM analyses and processing of the surface images, respectively. Centro Nacional de Pesquisa em Energia e Materiais (CNPEM) and Centro de Caracterização e Desenvolvimento de Materiais (CCDM) are also recognized for their support.

References

1 M. D. Salazar and M. Ratnam, *Cancer Metastasis Rev.*, 2007, **26**, 141.
2 L. Liu, X. Zhu, D. Zhang, J. Huang and G. Li, *Electrochem. Commun.*, 2007, **9**, 2547.
3 K. D. Bhalerao, S. C. Lee, W. O. Soboyejo and A. B. O. Soboyejo, *J. Mater. Sci.: Mater. Med.*, 2007, **18**, 3.
4 G. Acharya, C. L. Chang, D. D. Doorneweerd, E. Vlashi, W. A. Henne, L. C. Hartmann, P. S. Low and C. A. Savran, *J. Am. Chem. Soc.*, 2007, **129**, 15824.
5 J. Weng, Z. Zhang, L. Sun and J. A. Wang, *Biosens. Bioelectron.*, 2011, **26**, 1847.
6 K. Tsukagoshi, N. Jinno and R. Nakajima, *Anal. Chem.*, 2005, **77**, 1684.
7 M. S. Wilson and W. Nie, *Anal. Chem.*, 2006, **78**, 6476.
8 N. V. Panini, G. A. Messina, E. Salinas, H. Fernández and J. Raba, *Biosens. Bioelectron.*, 2008, **23**, 1145.
9 S. Choi and J. Chae, *Biosens. Bioelectron.*, 2009, **25**, 118.
10 Y. K. Chung, J. Reboud, K. C. Lee, H. M. Lim, P. Y. Lim, K. Y. Wang, K. C. Tang, H. Ji and Y. Chen, *Biosens. Bioelectron.*, 2011, **26**, 2520.
11 W. K. T. Coltro, E. Piccin, E. Carrilho, D. P de Jesus, J. A. F. da Silva, H. D. T. Silva and C. L. do Lago, *Quim. Nova*, 2007, **30**, 1986.
12 M. Mascini and S. Tombelli, *Biomarkers*, 2008, **13**, 637.
13 W. K. T. Coltro, R. S. Lima, T. P. Segato, E. Carrilho, D. P. de Jesus, C. L. do Lago and J. A. F. da Silva, *Anal. Methods*, 2012, **4**, 25.
14 I. E. Tothill, *Semin. Cell Dev. Biol.*, 2009, **20**, 55.
15 W. K. T. Coltro, E. Carrilho and J. A. F. da Silva, *Biosensors and Bioelectronics*, 2012, submitted.
16 R. S. Lima, T. P. Segato, A. L. Gobbi, W. K. T. Coltro and E. Carrilho, *Lab Chip*, 2011, **11**, 4148.
17 A. Ulman, *Chem. Rev.*, 1996, **96**, 1533.
18 J. S. Andresa, L. M. Moreira, J. L. Magalhães, E. P. Gonzalez, R. Landers and U. P. Rodrigues-Filho, *Surf. Interface Anal.*, 2004, **36**, 1214.
19 J. L. Magalhães, L. M. Moreira, U. P. Rodrigues-Filho, M. J. Giz, M. A. Pereira-da-Silva, R. Landers, R. C. G. Vinhas and P. A. P. Nascente, *Surf. Interface Anal.*, 2002, **33**, 293.
20 G. M. Ingo, N. Zacchetti, D. D. Sala and C. Coluzza, *J. Vac. Sci. Technol., A*, 1989, **7**, 3048.
21 J. F. Moulder, W. F. Stickle, P. E. Sobol and K. D. Bomben, *Handbook of X-ray photoelectron spectroscopy*, Perkin-Elmer Corporation, 1992.
22 N. Guerroani, A. Baldo, T. Maarouf, A. M. Belu, C. M. Kassis and A. Mas, *J. Fluorine Chem.*, 2007, **128**, 925.
23 H. J. Martin, K. H. Schulz, J. D. Bumgardner and K. B. Walters, *Langmuir*, 2007, **23**, 6645.
24 H. Randhawa, *Thin Solid Films*, 1991, **196**, 329.
25 W. K. T. Coltro, J. A. F. da Silva and E. Carrilho, *Electrophoresis*, 2008, **29**, 2260.
26 D. L. Nelson and M. M. Cox, *Lehninger Principles of Biochemistry*, New York: Worth Publishers, 3rd ed. 2000.
27 P. Gründler, *Chemical Sensors: An Introduction for Scientists and Engineers*, Berlin: Springer, 2007.
28 A. Escosura-Muñiz, A. Ambrosi and A. Merkoçi, *TrAC, Trends Anal. Chem.*, 2008, **27**, 568.
29 J. H. Kim, J. H. Cho, G. S. Cha, C. W. Lee and S. W. Paek, *Biosens. Bioelectron.*, 2000, **14**, 907.
30 S. J. Park, T. A. Taton and C. A. Mirkin, *Science*, 2002, **295**, 1503.
31 Y. Fan, X. Chen, J. Kong, C. Tung and Z. Gao, *Angew. Chem., Int. Ed.*, 2007, **46**, 2051.
32 J. Tanyanyiwa and P. C. Hauser, *Anal. Chem.*, 2002, **74**, 6378.
33 C. Y. Lee, C. M. Chen, G. L. Chang, C. H. Lin and L. M. Fu, *Electrophoresis*, 2006, **27**, 5043.
34 Y. Xu, J. Liang, H. Liu, X. Hu, Z. Wen, Y. Wu and M. Cao, *Anal. Bioanal. Chem.*, 2010, **397**, 1583.
35 K. A. Mahabadi, I. Rodriguez, C. Y. Lim, D. K. Maurya, P. C. Hauser and N. F. Rooij, *Electrophoresis*, 2010, **31**, 1063.
36 J. A. F. da Silva and C. L. do Lago, *Anal. Chem.*, 1998, **70**, 4339.
37 J. Lichtenberg, N. F. de Rooij and E. Verpoorte, *Electrophoresis*, 2002, **23**, 3769.
38 F. Laugere, R. M. Guijt, J. Bastemeijer, G. van Der Steen, A. Berthold, E. Baltussen, P. Sarro, G. W. K. van Dedem, M. Vellekoop and A. Bossche, *Anal. Chem.*, 2003, **75**, 306.
39 K. J. M. Francisco and C. L. do Lago, *Electrophoresis*, 2009, **30**, 2009.
40 G. Fercher, A. Haller, W. Smetana and M. J. Vellekoop, *Anal. Chem.*, 2010, **82**, 3270.
41 B. Liu, Y. Zhang, D. Mayer, H. J. Krause, Q. Jin, J. Zhao and A. Offenhäusser, *Electrophoresis*, 2011, **32**, 699.